ICRIE 2023 4th INTERNATIONAL CONFERENCE ON RECENT INNOVATIONS IN ENGINEERING

Proceedings of the 4th International Conference on Recent Innovation in Engineering
ICRIE 2023, University of Duhok, College of Engineering, 13th – 14th September 2023
(Special issue for Passer journal of basic and applied sciences)
Paper No. 01

Full P Seismic Performance Assessment of Reinforced Concrete Buildings Using Collapse Fragility Curve aper Title in Title Case

Ali ALRAWAS[1,*], Reem ALSEHNAWI[2]
[1]Higher Institute of Earthquake Studies&Researches, University of Damascus, Syria
[2]Higher Institute of Earthquake Studies&Researches, University of Damascus, Syria
* Corresponding author:[1]Higher Institute of Earthquake Studies&Researches, University of Damascus, Syria. Tel: +963993830473.
ali.arw@damascusuniversity.edu.sy: reem1.salman@damascusuniversity.edu.sy

ABSTRACT

Obtaining a collapse fragility curve is essential for loss estimation and structural safety studies, especially for vital facilities such as health centres. Many methods have been presented to develop fragility curves, such as the analytical method, which involves performing a series of nonlinear dynamic analyses, and empirical methods. This paper presents a study on the seismic performance assessment against the collapse of code-compliant reinforced concrete buildings. The study was carried out at Al-Qutayfah Hospital, located in a moderate seismicity area in Rif Dimashq, Syria. This hospital is representative of many modern hospitals built after 2004. A 3D analytical model was created using CSI-PERFORM 3D. The shear wall cross-section was modelled as a fibre section and a concentrated hinge for the frames to capture the essential nonlinear behaviour of the main elements and the potential collapse mode. An incremental dynamic analysis was performed using 11 pairs of ground motion records in accordance with FEMA P-58 recommendations to derive the collapse fragility and compare it to another result that converts the static pushover curve to an incremental dynamic analysis curve using the Vamvatsikos & Cornell method known as SPO2IDA. The results showed that the building had a low and acceptable probability of collapse under the code-defined MCE intensity level and that the SPOTOIDA method provides a reliable estimate of collapse fragility, saving time and effort.

KEYWORDS: Collapse; Fragility Curve; Incremental dynamic analysis; Seismic hazard; Reinforced concrete buildings

1 INTRODUCTION

This study was part of the seismic performance assessment of a modern RC hospital in Rif-Dimashq, designed according to the Syrian Arab Code for the Design and Implementation of Reinforced Concrete Structures - Loads on Buildings, 2005. As known, modern assessment methods such as Fema P-58 time-based assessment method help in estimating the probable performance of the building over time, considering all possible earthquakes and their probability of occurrence and estimating the losses Fema P-58 (2018), while the equivalent static design method doesn't ensure that the performance of both structural and non-structural components of the building is acceptable even with unjustified overestimated demands on the structure such as increasing base shear. In the literature, many studies have investigated the collapse fragility of shear wall buildings. Bilgin (2015) investigated the effect of material and construction quality on the collapse fragility of three RC hospitals in Turkey. Dabaghi et al. (2019) generated collapse fragility curves for RC shear wall buildings with different heights, wall dimensions and transverse confinement spacing. Zhong et al. (2022) proposed a new method called site-specific adjustment framework for

incremental dynamic analysis, which enables the use of incremental dynamic analysis in site-specific seismic risk analysis. Locally, there are no studies for the assessment of existing hospitals. Therefore, this research deals with the collapse fragility of the building, which was considered as a main step in the probable performance assessment process. In this study, we focused more on the nonlinear modelling of the main structural components of the building and the evaluation of the seismic hazards for the performance assessment to be presented later.

2 FRAGILITY FUNCTION

The fragility function specifies the probability of collapse or some other performance level as a function of the ground motion intensity measure (IM) (Baker 2015). The IM is usually taken as the 5% damped response spectral acceleration at the first mode period or peak ground acceleration (PGA). A lognormal cumulative distribution function is commonly used to define the fragility function (Porter et al. 2007). Where **Equation (1)** refers to the probability of collapse at a given intensity, event C refers to the collapse, Φ is the normal distribution, θ and β are the median and standard deviation, respectively.

$$P\left(C \mid IM = x\right) = \Phi\left(\frac{\ln\left(x/\theta\right)}{\beta}\right) \quad (1)$$

There have been many approaches to derived fragility functions, such as judgement, but the most common are the so-called analytical methods involving structural analysis, such as incremental dynamic analysis IDA (Vamvatsikos and Cornell 2002) or multiple stripe analysis (MSA) (Jalayer 2003).

IDA involves performing a large number of nonlinear response history analyses using a set of ground motions systematically scaled from the intensity at which the building response is elastic to the intensity at which all motions cause collapse (Vamvatsikos and Cornell 2002). In this case, the median of the fragility curve was calculated using **Equation (2)**. The main problem with IDA is that it is very time-consuming and, in some cases, scaling the ground motions by a large factor to produce high intensities is unreasonable and obtaining the collapse probability under a very high intensity isn't always useful. Another method is multiple stripe analysis, where the analysis has been performed on several IM levels, usually ten or eight, and each level has its ground motions, and not all motions need to cause collapse; MSA is more efficient and saves much time and allows more variability in ground motions (Jalayer 2003).

$$\ln\theta = \frac{1}{n}\sum_{i=1}^{n}\ln IM_i \quad (2)$$

It's well known that it's difficult to analytically determine building collapse where there is no single definition of collapse (Villaverde 2007); many codes and building standards have different collapse definitions and criteria. For example, Eurocode 8 uses local engineering demand parameters (EDD) where collapse occurs when the deformation or force demand on some elements exceeds specified limits, other codes such as Fema 356 use global EDB where collapse occurs when the inter-story drift ratio (IDR) exceeds 4%. In some cases, using global EDB collapse criteria doesn't give accurate results, so a combination of global and local EDB could be used. Also, collapse criteria depend on the structural analysis and the type of the building's structural system; Camata et al. use a roof drift ratio (RDR) corresponding to a 50% capacity drop after the peak of the pushover curve as the collapse criteria for infill frame buildings (Camata et al. 2017). On the other hand, when IDA is used, collapse occurs when the IDA curves are flattened, or their slope is less than 20% of the elastic slope (Fema P-58 2018). According to Fema P-58 (2018), when using IDA, the collapse occurs when the demand on the gravity-carrying components exceeds their capacity when numerical instability occurs or when the IDA curve gets flattered; Kim and Foutch found that the flattered of the IDA curve is not appropriately applicable to shear wall buildings This is attributed to the large lateral stiffness of shear wall buildings and the P-delta effect on low and mid-rise shear wall buildings is so small; moreover, shear walls yield very quickly, and the building can achieve stable behaviour even when the IDA curve gets flattered, and the gravity system collapse starts from 5.8%

drift (Kim and Foutch 2007). In this study, the collapse of vertical members was assumed to occur at 5% IDR.

3 CASE-STUDY DEFINITION

This study was conducted on Al-Qutayfah Hospital serving nearby cities; the hospital consisted of two buildings separated by 10cm gab; the main building consisted of five stories and a basement with a floor height of 3.9m for all floors and 845m^2 area. The second building is two stories with a basement and an area of 545m^2. The building was designed according to the Syrian Arab Code for the Design and Implementation of Reinforced Concrete Structures - Loads on Buildings, 2005. Only the first building was investigated, as the second building "to the right of the main building in **Figure 1**" doesn't affect the dynamic response of the investigated building. **Figure 1** shows the architectural plan for the ground floor, and **Figure 2** shows only the columns and shear walls used in the model.

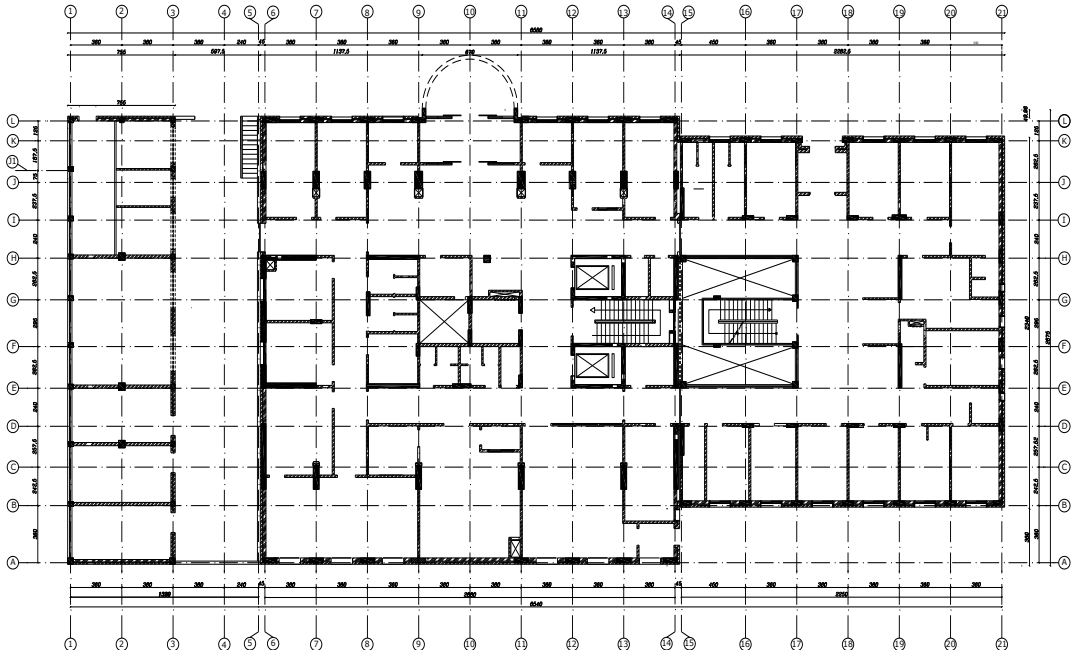

Figure 1: Ground stories plane, some non-structural elements were deleted for clarity.

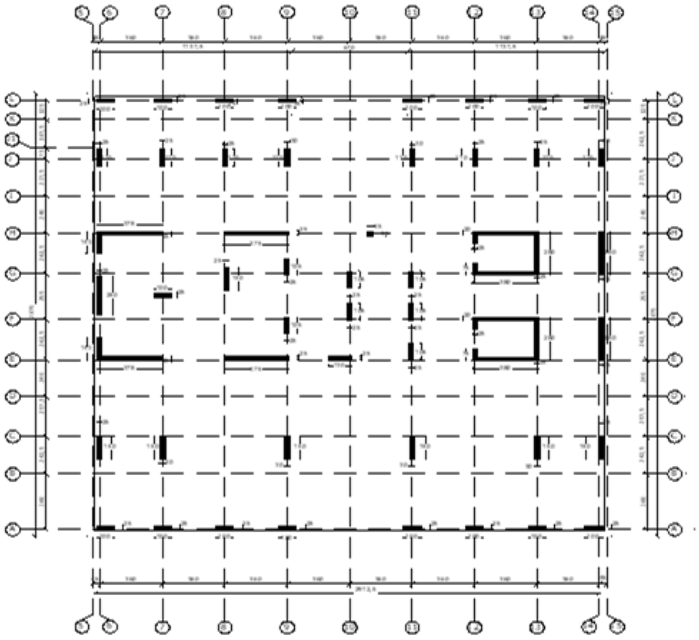

Figure 2: Columns and shear walls plane for the first structure.

4 NONLINEAR MODELING

CSI Perform 3D was used to create a mathematical model of the structural elements, neglecting the contribution of infill walls to lateral stiffness. Shear walls are modelled in Perform 3D using 4 nodes of macro elements with 6 degrees of freedom (DOF) for each node, 3 rotational and 3 transitional (Lowes et al. 2018). Out-of-plane flexural and shear behaviours are elastic, defined by Young's modulus passion ratio and a reasonable thickness that is not too small for the program to detect buckling. In-plane bending behaviour is simulated using the fibre cross-section. In-plane shear behaviours were simulated using a uniform linear shear layer (Lowes et al. 2018).

CSI Perform 3D, using the YULRX backbone model, is shown in **Figure 3** to define the envelope of the stress-strain or force-deformation curve for material and component behaviour. This study follows the recommendations of Lowes et al. (2018) for slender shear wall modelling, where Lowes et al. used liberation experiments on eight planer slender concrete shear walls to develop recommendations for more accurate and relevant modelling. The stress-strain fibre parameters for unconfined and confined concrete were taken as recommended in the previous work, with the Mander et al. (1988) model used for confined concrete to define the confinement effect and **Equation (3)** from Paulay and Priestley (1998) for concrete strain capacity, where ρ_h is the volumetric confinement steel ratio f_{yh} yield strength at the maximum strength of the transverse steel.

$$\varepsilon_{c\max} = 0.004 + \rho_h f_{yh} \varepsilon_{hm} / f_{cc}^{'} \qquad (3)$$

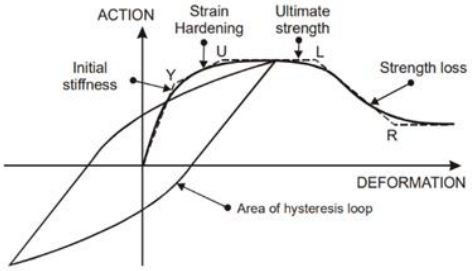

Figure 3: Basic YULRX backbone curve in Perform 3d (Perform 3D Components and Elements v9 2022).

For horizontal mesh, four elements per wall were used, two for the boundary zone and two for the rest of the wall, due to the highly nonlinear longitudinal strain distribution along the wall (Lowes et al. 2018). For the vertical mesh, four elements were used per floor, and to generate the mesh-free model, the material model for both confined and unconfined concrete was regularized by modifying the value of the strain at point R using **Equations (4)** and **(5),** where Lelem is the element length equal to one-quarter of the floor height, G_{fc} and G_{fcc} are the unconfined and confined concrete crushing energies, respectively, using **Equations (6)** and **(7).**

$$\varepsilon_R = \varepsilon_{} - \frac{f_c^{'}}{E_c} + 2\frac{\left(\frac{G_{fc}}{Lelem}\right)}{f_c^{'}} \quad (4)$$

$$\varepsilon_{Rcc} = \varepsilon_0 - \frac{0.8 f_{cc}^{'}}{E_{cc}} + \frac{\frac{5}{3}\left(\frac{G_{fcc}}{Lelem}\right)}{f_c^{'}} \quad (5)$$

$$G_{fc} = 0.5 Kip/in \quad (6)$$

$$G_{fcc} = 0.5 \le 2.5\left(\frac{f_{cc}^{'}}{f_c^{'}} - 0.85\right) \le 2.5 \quad (7)$$

For in-plane effective bending stiffness, the value $0.5E_cA_g$ was used as recommended in ASCE/SEI 41 for in-plane effective bending rigidity, and 0.25 of $G=E_c/2(1+v)$ for effective shear stiffness.

Frame elements were modelled using the lumped plasticity approach, so a zero-length nonlinear hinge was used at each element end. For beams, the M-θ rotational hinge parameters were based on the work of Haselton et al. (2016). This model can simulate the response of the hinge under large displacements up to lateral collapse. For columns, P-M-M hinges are also assigned to each column end. The M-θ backbone is shown in **Figure 4**. The parameters of the hinge were calculated from **Equations (8)** to **(10),** and to account for cyclic degradation, both θ_{cap}, p_l and θ_{pc} are reduced using **Equations (11)** and **(12)**, where v is the axial load ratio, ρ_{sh} is the transverse reinforcement ratio, and asl is equal to 1. M_y is taken as the nominal moment strength calculated using the expected material strength. In our model, we assume that the strength didn't fall to zero; instead, we take the residual strength to be 0.2 of the peak strength M_c.

$$M_c / M_y = 1.13 \quad (8)$$

$$\theta_{cap,pl} = 0.10\left(1+0.55a_{sl}\right)\left(0.16\right)^{\nu}\left(0.02+40\rho_{sh}\right)^{0.43}\left(0.54\right)^{0.01 f_c'} \quad (9)$$

$$\theta_{pc} = \left(0.78\right)\left(0.031\right)^{\nu}\left(0.02+40\rho_{sh}\right)^{1.02} \le 0.1 \quad (10)$$

$$\theta_{cap,pl,cyclic} = 0.7\theta_{cap,pl} \quad (11)$$

$$\theta_{pc,cyclic} = 0.5\theta_{pc} \quad (12)$$

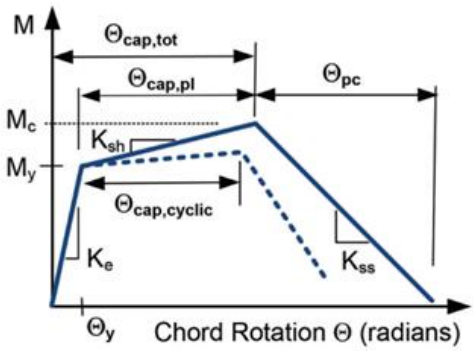

Figure 4: Moment-rotation backbone parameters (Haselton et al. 2016).

For the lateral stiffness of RC frame elements, the main contribution comes from flexural and beam slip deformations; the shear deformation contribution could be neglected (NIST 2017a). To calculate the effective flexural stiffness of beams and columns, we used the Kwon **Equation (13)**, where the effective lateral stiffness is related to the compressive axial load ratio, the peak drift ratio (DR), and ρ_T is the longitudinal tensile steel reinforcement ratio (Kwon and Ghannoum 2016).

$$\frac{E_c I_{eff}}{E_c I_g} = 0.003DR^{-0.65} + \gamma \le 0.8DR \le 0.012$$

$$\gamma = \left(-50\rho_T + 2.5\right)\left(\frac{P}{A_g f_c'}\right)^{\left(-20\rho_T+2.15\right)} + \left(15\rho_T + 0.05\right) \quad (13)$$

To save analysis time, and because the building doesn't have in-plane and out-of-plane offset irregularities and membrane discontinuity irregularities, the rigid membrane assumption with kinematic constraint was used.

To simulate the response of the foundation system and the soil and its effect on increasing or decreasing the demand level on the model, NIST (2017b) suggests that if the structure-to-soil stiffness ratio in **Equation (14)** is less than 0.1, the soil-structure interaction can be neglected. In our case, the ratio is less than 0.1, so the fixed-base model was considered.

$$R = \frac{h}{V_s T} \quad (14)$$

H here is building high, T is the structure fixed-base period, and Vs is the shear-wave velocity of soil.

The damping ratio is 4% for the period range 1.0T1-0.2T1, where T1 is the first mode period, the first two transition periods are 0.88 and 0.57 sec, respectively, and the code-based period is

0.52 sec. The gravity load is the total dead load plus half the live load, and the lateral seismic load is the dead load only. **Figure 5** shows the model in Perform 3D.

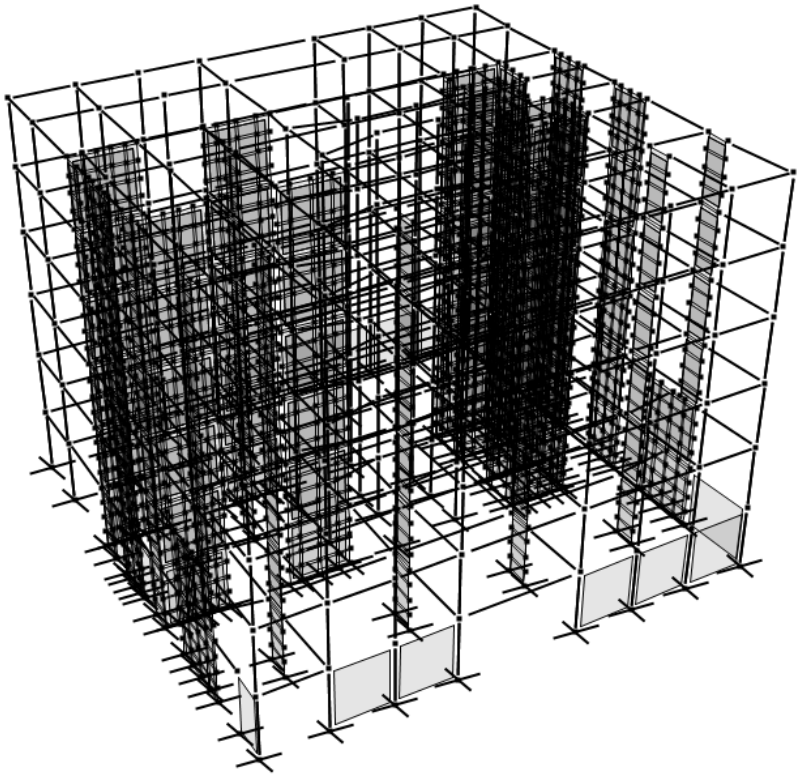

Figure 5: mathematical model of the building in Perform 3D.

5 SEISMIC HAZARD

The building is located in an area of moderate seismicity (2C zone) where the deterministic PGA is 0.25g according to the Syrian Arab Code for the Design and Implementation of Reinforced Concrete Structures-Loads on Buildings in 2005. **Figure 6** shows a seismic hazard map of Syria (Ssayed et al. 2012), **Figure 7** shows the Uniform Hazard Spectrum (UHS) for the location and selection of ground motions, and **Figures 8** and **9** show the disaggregation diagram for 0.01 and 0.7 sec.

To perform IDA, Fema P-58 (2018) requires a minimum of 11 pairs of ground motions, each rotated 90 degrees to produce 22 motion sets. To select and scale ground motions, UHS was used instead of Conditional Mean Spectrum (CMS) (Baker 2010). Initially, the spectral mean collapse capacity was estimated as 3 times the code elastic design level at 0.7 s, approximately 1.75 g, as the building was designed to confirm the seismic requirements of the building code. $(T)^{-}$ equal to the average of the periods of the fundamental mode of translation along each of two orthogonal building axes, then from the hazard curve of 0.7 sec period, the period of return for was estimated and developed UHS consisted with the previous hazard level and using it as the target spectra. From the deaggregation data, the magnitude and epicentre distance used for selection is and **Figure 10** shows target spectra with mean spectra of selected motions and with individual spectra, and **Table 1** lists selected ground motions.

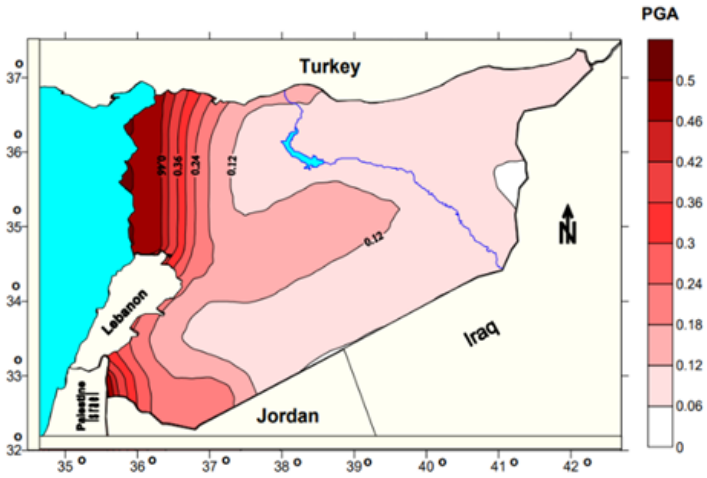

Figure 6: Seismic hazard map of Syria, distribution of PGA for return period of 1000 years (Ssayed et al. 2012).

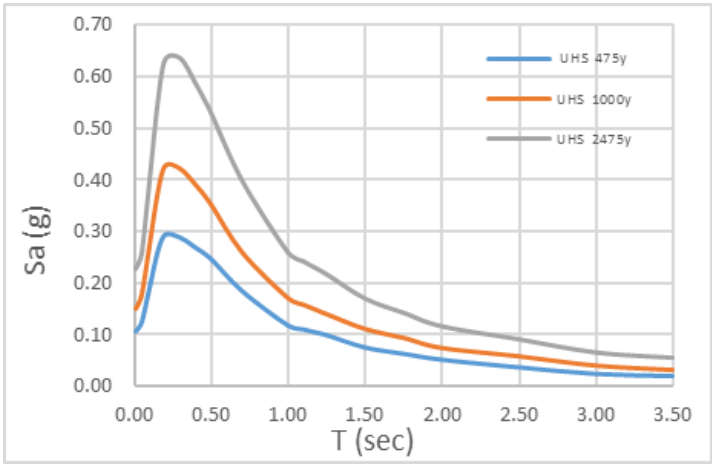

Figure 7: UHS for 475, 1000, and 2475-year periods of return.

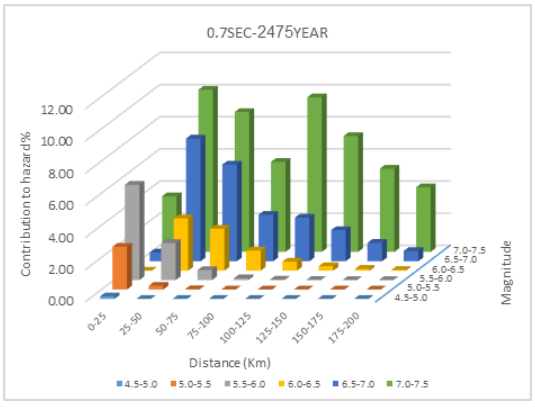

Figure 8: Disaggregation chart for 0.01sec for 2475 years of return.

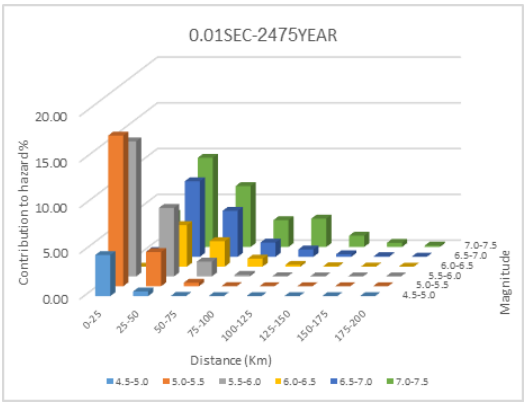

Figure 9: Disaggregation chart for 0.7sec for 2475 years of return.

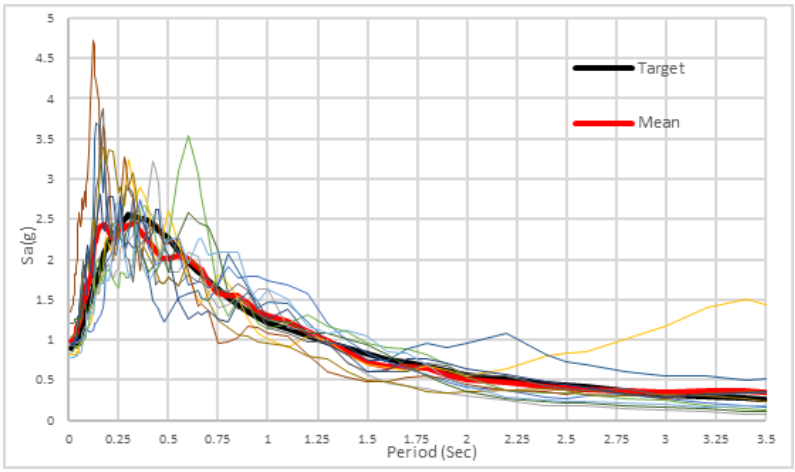

Figure 10: Target means and individual spectra of selected ground motions used in the study.

Table 1: List of ground motion properties.

RSN	MSE*	SF**	5-75% Sec	5-95% Sec	Earthquake Name	Rrup (km)	Vs30 (m/sec)	Magni-tude
902	0.02	4.70	6.40	12.10	"Big Bear-01"	40.54	359	6.46
1634	0.02	4.88	16.20	23.30	"Manjil_ Iran"	75.58	302.64	7.37
1794	0.04	5.72	7.40	14.60	"Hector Mine"	31.06	379.32	7.13
3756	0.05	5.15	23.00	32.90	"Landers"	40.67	368.2	7.28
5832	0.10	4.40	28.30	46.30	"El Mayor_ Mexico"	26.55	242.05	7.2
5836	0.09	3.73	11.20	24.70	"El Mayor_ Mexico"	29	264.57	7.2
5988	0.06	3.87	21.40	68.60	"El Mayor_ Mexico"	30.63	196	7.2
5990	0.08	4.17	17.70	42.50	"El Mayor_ Mexico"	27.91	210.51	7.2
6013	0.03	4.86	15.70	65.80	"El Mayor_ Mexico"	28.3	276.25	7.2
6877	0.03	4.12	5.10	11.20	"Joshua Tree_ CA "	25.53	292.12	6.1
6971	0.04	4.86	16.10	22.70	"Darfield_ New Zea-land"	29.86	389.54	7

*MSE is mean square root error. ** SF is the used scale factor.

6 ANALYSIS RESULTS

IDA and pushover analyses were performed. **Figure 11** shows the IDA curve, with spectral acceleration at 0.7 sec selected as the intensity measure and IDR as the demand parameter, and structural collapse assumed at 5% IDR. The fragility curve **(Table 1)** was fitted using a lognormal distribution with

a mean of 2.8g and a dispersion of 0.5, assuming the average quality of the analytical model and for quality assurance of the design.

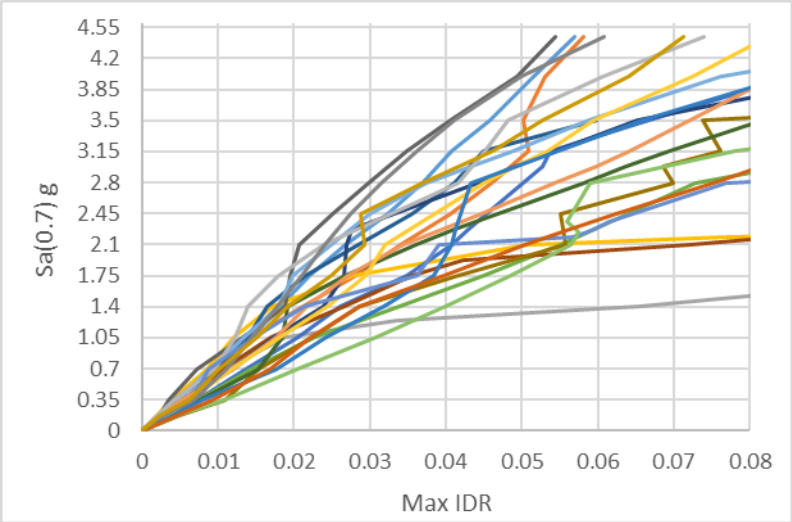

Figure 11: Incremental dynamic analysis curves.

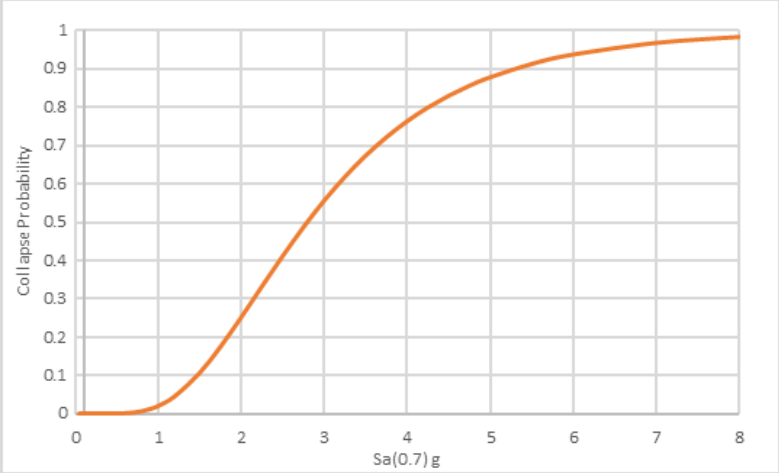

Figure 12: Collapse fragility curve.

Pushover analysis was carried out in X and Y directions with modal force distribution. **Figures 13** and **14** show the static pushover (SPO) curve. In the X-direction, a sudden drop in the curve was related to the torsional effect and the limited deformation capacity of the columns due to the low transverse reinforcement ratio. Using the Static Pushover to Incremental Dynamic Analysis (SPO2IDA) Excel workbook (Vamvatsikos and Cornell 2006) to generate the 16th, 50th (median) and 84th IDA curves (**Figures 15** and **16**) and then using the spectral acceleration at the collapse of 2.91 g as the mean value for the fragility function (**Figure 17**) with a dispersion of 0.6 as recommended by Fema P-58.

7 COLLAPSE PROBABILITY ASSESSMENT

Using the collapse fragility curve resulting from IDA, the collapse probability under the code-defined MCE intensity level $S_a(0.52)$ =1.2g was approximately 5.3%. Here, the code's approximate period of 0.52

s was used instead of a dynamic period, as it is more conservative and more common in practice. The probability of collapse using the fragility curve obtained with SPO was 8%. For health centres, a collapse probability of 5% under the MCE intensity level is acceptable as the seismic hazard map of the Syrian Arab Code for the Design and Implementation of Reinforced Concrete Structures-Loads on Buildings in 2005 tends to overestimate seismic hazards (Ssayed 2012). The use of a 5% drift limit as a collapse criterion is also a conservative assumption.

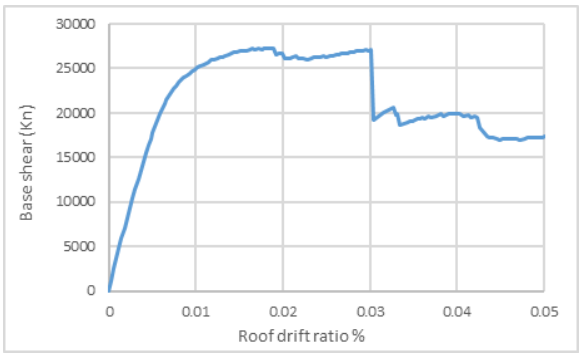

Figure 13: SPO curve at +X direction.

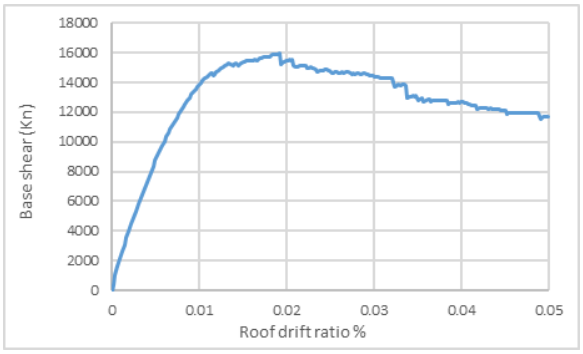

Figure 14: SPO curve at +Y direction.

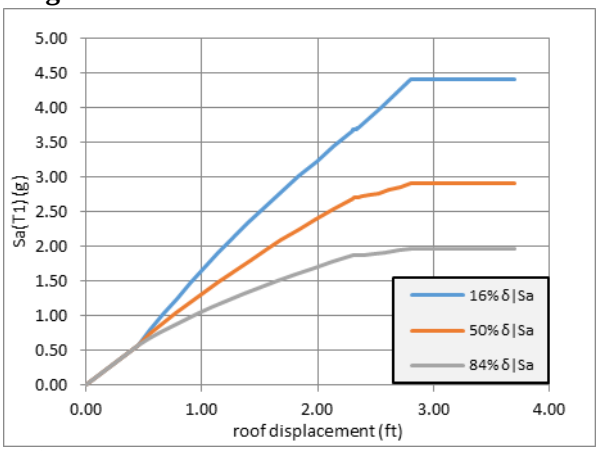

Figure 15: IDA curve using SPO2IDA at X direction

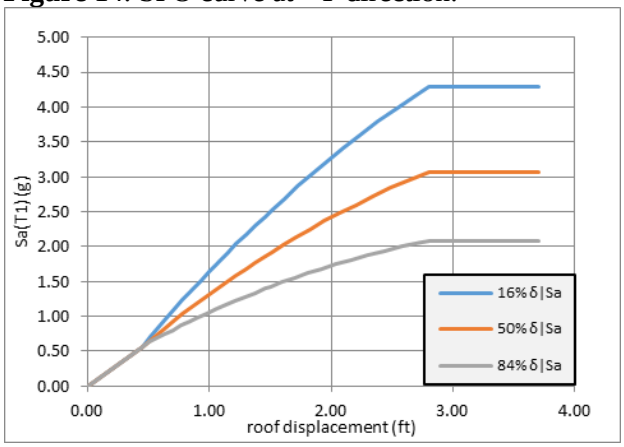

Figure 16: IDA curve using SPO2IDA in Y direction

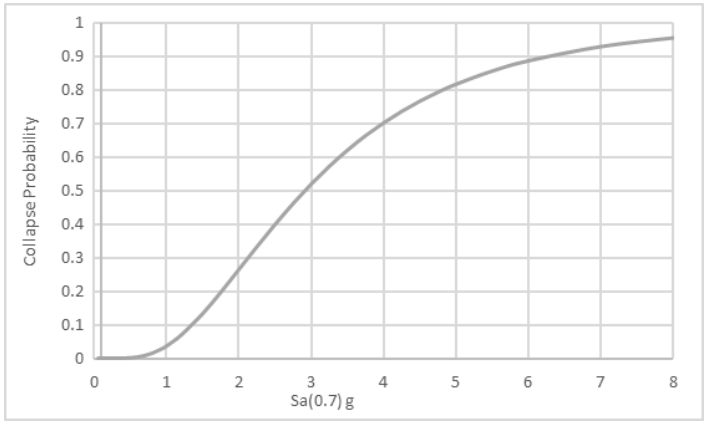

Figure 17: collapse fragility curve.

8 CONCLUSION

The objective of this paper was to derive the structural collapse fragility IDA for a code-compliant RC building. A numerical model for the building was modelled using Perform-3D, implying a fibre section for shear walls and concentrated M-θ and P-M-M hinges for beams and columns. The probabilistic seismic hazard analysis was performed to generate the UHS and the disaggregation data to select and scale the ground motions; then, IDA was performed, and collapse was assumed to occur at 5%, corresponding to the collapse of the gravity system. The result showed that the structure has an acceptable and low probability of collapse under a code-defined MCE intensity level.

REFERENCES

1. Baker JW (2010) Conditional mean spectrum: a tool for ground-motion selection. J Struct Eng 137(3):322–331
2. Baker, J. W., (2015). Efficient analytical fragility function fitting using dynamic structural analysis, Earthquake Spectra 31, 579–599.
3. Bilgin, Huseyin. (2015). Generation of Fragility Curves for Typical RC Health Care Facilities: Emphasis on Hospitals in Turkey. Journal of Performance of Constructed Facilities. 30. 10.1061/(ASCE)CF.1943- 5509.0000806.
4. Camata G, Celano F, De Risi MT, Franchin P, Magliulo G, Manfredi V, Masi A, Mollaioli F, Noto F, Ricci P, Spacone E, Terrenzi M, Verderame G (2017) RINTC project: nonlinear dynamic analyses of Italian code-conforming reinforced concrete buildings for risk of collapse assessment. In: COMPDYN 2017—6th ECCOMAS thematic conference on computational methods in structural dynamics and earthquake engineering, Rhodes Island, pp 15–17
5. Dabaghi, M., Saad, G. and Allhassania, N., (2019). Seismic Collapse Fragility Analysis of Reinforced Concrete Shear Wall Buildings. Earthquake Spectra, 35(1), pp.383-404.
6. Federal Emergency Management Agency (FEMA), (2018). Seismic Performance Assessment of Buildings, Volume 1 – Methodology, Second Edition, FEMA P-58-2, Federal Emergency Management Agency, Washington, D.C.
7. Haselton, C. B., Liel, A. B., Taylor-Lange, S. C., & Deierlein, G. G. (2016). Calibration of Model to Simulate Response of Reinforced Concrete Beam-Columns to Collapse. ACI Structural Journal, 113(6).
8. Jalayer, F. (2003). Direct Probabilistic Seismic Analysis: Implementing Nonlinear Dynamic Assessments. Ph.D. Thesis, Dept. of Civil and Environmental Engineering, Stanford University, Stanford, CA.
9. Kim, T., and Foutch, D. A., (2007). Application of FEMA methodology to RC shear wall buildings governed by flexure, Engineering Structures 29, 2514–2522.
10. Kwon, J., and Ghannoum, W.M., (2016), "Assessment of international standard provisions on the stiffness of reinforced concrete moment frame and shear wall buildings," Engineering Structures, Vol. 128, pp. 149-60.
11. Lowes, Laura & Baker, Carson. (2018). Recommendations for Modeling the Nonlinear Response of Slender Reinforced Concrete Walls Using PERFORM-3D.
12. Mander, J.B., Priestley, M.J.N., Park, R. (1988). "Observed Stress-Strain Behaviour of Confined Concrete," Journal of Structural Engineering, ASCE 114(8): 1827-1849.

13. National Institute of Standards and Technology (NIST). (2017). Guidelines for nonlinear structural analysis and design of buildings. part IIb - reinforced concrete moment frames.
14. National Institute of Standards and Technology (NIST). (2017). Guidelines for Nonlinear Structural Analysis and Design of Buildings Part I – General.
15. Paulay, T., Priestley, M.J.N. (1992). Seismic Design of Reinforced Concrete and Masonry Buildings. John Wiley and Sons.
16. Porter, K., Kennedy, R., and Bachman, R., 2007. Creating fragility functions for performance based earthquake engineering, Earthquake Spectra 23, 471–489.
17. Ssayed, H. M. E., Zaineh, H., Dojcinovski, D., & Mihailov, V. (2012). Re-Evaluations of Seismic Hazard of Syria. International Journal of Geosciences, 03(04), 847–855.
18. Terrenzi, M., Spacone, E., & Camata, G. (2018). Collapse limit state definition for seismic assessment of code-conforming RC buildings. International Journal of Advanced Structural Engineering, 10(3), 325–337.
19. Vamvatsikos, D., and Cornell, C. A., (2002). Incremental dynamic analysis, Earthquake Engineering & Structural Dynamics 31, 491–514.
20. Vamvatsikos, D., and Cornell, C.A., (2006), Direct estimation of the seismic demand and capacity of oscillators with multi-linear static pushovers through IDA, Earthquake Engineering and Structural Dynamics, Vol. 35, Issue 9, pp. 1097-1117
21. Villaverde R (2007) Methods to assess the seismic collapse capacity of building structures: state of the art. J Struct Eng 133(1):57–66
22. Zhong, K., Chandramohan, R., Baker, J. W., & Deierlein, G. G. (2022). Site-specific adjustment framework for incremental dynamic analysis (SAF-IDA). *Earthquake Spectra*. https://doi.org/10.1177/87552930221083688